Title	Intersubband polaritons with spin-orbit interaction
Author(s)	Kyriienko, Oleksandr.; Shelykh, Ivan A.
Citation	Kyriienko, O., & Shelykh, I. A. (2013). Intersubband polaritons with spin-orbit interaction. Physical Review B, 87(7), 075446-.
Date	2013
URL	http://hdl.handle.net/10220/9915
Rights	© 2013 American Physical Society. This paper was published in Physical Review B and is made available as an electronic reprint (preprint) with permission of American Physical Society. The paper can be found at the following official DOI: http://dx.doi.org/10.1103/PhysRevB.87.075446. One print or electronic copy may be made for personal use only. Systematic or multiple reproduction, distribution to multiple locations via electronic or other means, duplication of any material in this paper for a fee or for commercial purposes, or modification of the content of the paper is prohibited and is subject to penalties under law.

Intersubband polaritons with spin-orbit interaction

O. Kyriienko and I. A. Shelykh
Science Institute, University of Iceland, Dunhagi 3, IS-107, Reykjavik, Iceland and
Division of Physics and Applied Physics, Nanyang Technological University 637371, Singapore
(Received 5 October 2012; revised manuscript received 10 December 2012; published 27 February 2013)

We investigate intersubband polaritons formed in the asymmetric quantum well embedded into the semiconductor microcavity and study the effects of spin-orbit interaction (SOI) acting on intersubband excitations. The spin-orbit interactions of Rashba and Dresselhaus type remove the spin degeneracy of electrons with finite value of in-plane momentum and allow four types of intersubband excitations. While optical spin-flip transitions are suppressed, the spectrum of elementary excitations shows the appearance of upper, lower, and middle polariton branches based on spin-conserving transitions. The accounting of finite photon momentum leads to nonzero average spin projection of electronic ensemble in the first excited subband under continuous wave excitation for both isotropic (Rashba) and anisotropic (Rashba and Dresselhaus) SOI. We predict the possibility of spin-current generation in the considered systems with long coherence length.

DOI: 10.1103/PhysRevB.87.075446 PACS number(s): 72.25.Fe, 71.36.+c, 78.67.De

I. INTRODUCTION

Intersubbband transition in the semiconductor quantum well (QW) plays a significant role in modern optoelectronics due to numerous possible applications in optical devices operating in the infrared and terahertz frequency domains.[1–4] The dependence of energy distance between subbands on QW width allows one to adjust the frequency of photon emitter or detector in a relatively easy way compared to the usual interband transition. Moreover, the implementation of multiple QW samples gives the possibility to create devices with high efficiency, in particular quantum cascade lasers.[5,6]

An important characteristic of intersubband transition as compared to interband transitions is the peculiar optical selection rules which only allow absorption of the transverse magnetic (TM) polarized electromagnetic mode because the dipole element of transition for the transverse electric (TE) polarized mode is zero.[7] Furthermore, it is possible to improve the efficiency of light interaction with absorbing media by placing it into the semiconductor microcavity. This allows one to achieve the strong-coupling regime when in the case of intersubband transition cavity photons are constantly absorbed and emitted and mixed light-matter modes are formed.[8–10]

Up to now, a consideration of the spin properties for intersubband polaritons was never performed. On the other hand, the spin electronics or *spintronics* is one of the most quickly developing areas of mesoscopic physics. The main issue of spintronics is spin transfer in the system and generation of spin currents. Being widely studied nowadays, it proposes the devices which operate on other principles compared to usual electronics,[11,12] for instance, the spin field effect transistor.[13]

One should note that contrary to the case of the intersubband polaritons, the spin properties of interband cavity polaritons were widely studied.[14] Moreover, by analogy with spintronics, its optical counterpart, *spinoptronics*, became recently an area of intensive studies.[15] In this domain, the role of Rashba spin-orbit interaction (SOI) is played by so-called TE-TM splitting,[16] and optical analogs of various spintronic components were theoretically proposed and experimentally realized.[17]

One of the basic concepts in spintronics is the spin-orbit interaction,[18,19] which appears in semiconductors due to intrinsic bulk inversion asymmetry (BIA) or structure inversion asymmetry (SIA).

The part of SOI appearing in the systems with structure inversion asymmetry, e.g., asymmetric quantum wells (AQW), is known as the Rashba term. It can be represented by introduction of the in-plane effective magnetic field which is momentum dependent and acts solely on electron spin causing its precession.[20] The corresponding Hamiltonian reads as

$$H_{\mathrm{SIA}} = \alpha(\sigma_x k_y - \sigma_y k_x) = \frac{\hbar}{2}(\mathbf{\Omega}_{\mathrm{SIA}} \cdot \boldsymbol{\sigma}), \tag{1}$$

where α is a Rashba SOI constant and $\mathbf{\Omega}_{\mathrm{SIA}} = 2\alpha\hbar^{-1}(k_y; -k_x)$ denotes the effective magnetic field (measured in frequency units) and $\boldsymbol{\sigma}$ is the Pauli matrix vector. The diagonalization of the electron Hamiltonian accounting for Rashba SOI modifies dispersions where two different spin components are split in energy for nonzero values of electron in-plane momenta. This removes the spin degeneracy in the system and makes possible effective spin control due to the possibility to tune the Rashba coupling parameter α by external gate voltage applied perpendicular to the structures' interface.[21–24]

Spin-orbit interaction arising from the bulk inversion asymmetry (BIA) is known as the Dresselhaus term. Similarly to the Rashba SOI, it leads to the appearance of linear in k effective magnetic field oriented in plane of the QW, but has different symmetry. The corresponding Hamiltonian can be written as[25]

$$H_{\mathrm{BIA}} = \beta(\sigma_x k_x - \sigma_y k_y) = \frac{\hbar}{2}(\mathbf{\Omega}_{\mathrm{BIA}} \cdot \boldsymbol{\sigma}), \tag{2}$$

where β is the Dresselhaus constant for material, $\mathbf{\Omega}_{\mathrm{BIA}} = 2\beta\hbar^{-1}(k_x; -k_y)$, and we consider the quantum well grown in the [001] direction. In realistic QWs, usually both types of spin splitting are present. This leads to a strongly anisotropic pattern of the effective magnetic field acting on electron spin in the reciprocal space.

In this paper, we study the effect of Rashba and Dresselhaus SOI on the intersubband optical transitions and formation of intersubband polaritonic states. Electrons in energy subbands

of asymmetric QW are subjected to SIA and BIA spin-orbit interaction, and both fundamental and upper subbands are spin split for $k \neq 0$. This opens four different optical transitions and allows us to form five different polaritonics states. In this paper, we show that optical transitions with spin flip are suppressed in the semiconductor microcavity, and spin-conserving excitations interacting with cavity photons give birth to three strongly coupled polaritonic modes with peculiar spin polarization. By tuning the pump conditions, one can generate the spin currents with long coherence length.

The paper is organized as follows. In Sec. II A, we present a Hamiltonian for intersubband excitation subjected to Rashba and Dresselhaus spin-orbit interaction. In Sec. II B, the possibility of optical spin orientation due to nonzero photon momentum is discussed. In Sec. II C, we discuss spin-current generation by linearly polarized light for intersubband transition. In Sec. III, we introduce the strong light-matter coupling in the system and show the spectrum of excitation with corresponding spin polarization of polaritonic modes. Finally, Sec. IV summarizes the results of the paper.

II. PHOTOABSORPTION OF INDIVIDUAL QW WITH SOI, SPIN POLARIZATION, AND SPIN CURRENTS

A. Model Hamiltonian

1. Rashba SOI

We consider a system of asymmetric GaAs/AlGaAs quantum wells embedded into the microcavity, where TM polarized cavity photons are confined [Fig. 1(a)]. The TE polarized mode can be excluded from consideration, as it is not coupled to intersubband transition in the dipole approximation. As compared to the case of symmetric rectangular quantum well, the asymmetry introduces Rashba spin-orbit interaction which induces the spin flips for the electrons moving with finite value of the momentum k.

The generic Hamiltonian for the considered system in the secondary quantization representation can be written as

$$H = \sum_{\boldsymbol{k},j,\sigma} E_{k,j} a^{\dagger}_{\boldsymbol{k},j,\sigma} a_{\boldsymbol{k},j,\sigma} + \sum_{\boldsymbol{k},j} \left[\alpha^{R}_{j}(k_y + ik_x) a^{\dagger}_{\boldsymbol{k},j,\uparrow} a_{\boldsymbol{k},j,\downarrow} + \text{H.c.}\right] + \sum_{\boldsymbol{q}} E^{\text{ph}}_{q} b^{\dagger}_{\boldsymbol{q}} b_{\boldsymbol{q}} + \sum_{\boldsymbol{k},\boldsymbol{q},\sigma} (g_q a^{\dagger}_{\boldsymbol{k},1,\sigma} a_{\boldsymbol{k}+\boldsymbol{q},2,\sigma} b^{\dagger}_{\boldsymbol{k}} + \text{H.c.}), \quad (3)$$

where we have chosen the axis perpendicular to the interface of the QW as spin quantization axis z. Here, $E_{k,j}$ and E^{ph}_{q} denote dispersion of electron in the subband j and cavity photon, respectively. $a^{\dagger}_{\boldsymbol{k},j,\sigma}, a_{\boldsymbol{k},j,\sigma}$ are creation and annihilation operators for electron with wave vector $\mathbf{k}$ and spin σ in the lower ($j = 1$) or upper ($j = 2$) subband, $b^{\dagger}_{\boldsymbol{q}}, b^{\dagger}_{\boldsymbol{q}}$ are creation and annihilation operators of the cavity photon. g_q is the electron-photon interaction constant which originates from the dipole matrix element of the intersubband transition and can

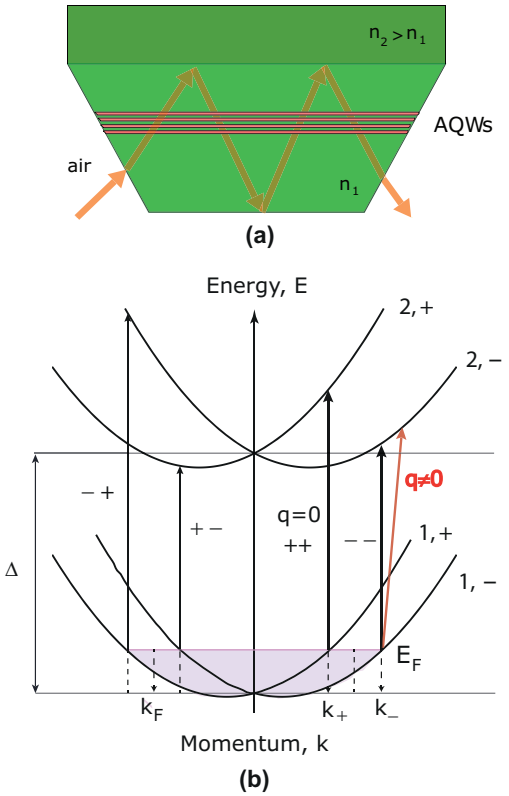

FIG. 1. (Color online) (a) Sketch of the geometry of the system. The set of asymmetric QWs is bounded into cavity formed due to the effect of total internal reflection (waveguide geometry). (b) The schematic representation of four possible transitions between upper and lower subbands split by SOI. Δ denotes bare transition energy, k_+ and k_- show the radii of Fermi surface for different SOI subbands.

be calculated as[10]

$$g_q = \sqrt{\frac{\Delta d^2_{21}}{\hbar^2 \epsilon \epsilon_0 L_{\text{cav}} A E^{\text{ph}}_{q}} \frac{q^2}{(\pi/L_{\text{cav}})^2 + q^2}}, \quad (4)$$

where L_{cav} is the cavity length, Δ is the separation energy between levels, ϵ_0 and ϵ are vacuum permittivity and material dielectric constant, respectively, d_{21} stands for the dipole matrix element of the transition, and A is an area of the sample.

The first term in Hamiltonian (3) describes free particles and the second term corresponds to the Rashba spin-orbit interaction, where α_j are Rashba coefficients for different subbands, $j = 1,2$. Note that in general $\alpha_1 \neq \alpha_2$.[24] This term contributes to the mixing of $\uparrow$ and $\downarrow$ states. The third term is the free cavity photon energy and the fourth one describes the interaction between photons and the intersubband transition which conserves the electrons' spin.

It is convenient to diagonalize the electronic part of the Hamiltonian (3) introducing the new operators of spin states $\tilde{\sigma} = +,-$ oriented perpendicular to the direction of the momentum $\mathbf{k}$,

$$c_{\boldsymbol{k},\pm} = \frac{1}{\sqrt{2}}[\pm i e^{-i\theta_{\boldsymbol{k}}} a_{\boldsymbol{k},\uparrow} + a_{\boldsymbol{k},\downarrow}], \quad (5)$$

where $\theta_{\boldsymbol{k}} = \arctan(k_y/k_x)$ is the angle between the radial vector $\mathbf{k}$ and the x axis. The Hamiltonian of the light-matter

coupling written in new operators reads as

$$\widetilde{H} = \sum_{\boldsymbol{k},j,\tilde{\sigma}} \widetilde{E}_{k,j,\tilde{\sigma}} c^{\dagger}_{\boldsymbol{k},j,\tilde{\sigma}} c_{\boldsymbol{k},j,\tilde{\sigma}} + \sum_{\boldsymbol{q}} E^{\mathrm{ph}}_{q} b^{\dagger}_{\boldsymbol{q}} b_{\boldsymbol{q}} + \sum_{\boldsymbol{k},\boldsymbol{q}} [g_{++}(\boldsymbol{k},\boldsymbol{q}) c^{\dagger}_{\boldsymbol{k},1,+} c_{\boldsymbol{k}+\boldsymbol{q},2,+} + g_{--}(\boldsymbol{k},\boldsymbol{q}) c^{\dagger}_{\boldsymbol{k},1,-} c_{\boldsymbol{k}-\boldsymbol{q},2,-} + g_{+-}(\boldsymbol{k},\boldsymbol{q}) c^{\dagger}_{\boldsymbol{k},1,+} c_{\boldsymbol{k}+\boldsymbol{q},2,-} + g_{-+}(\boldsymbol{k},\boldsymbol{q}) c^{\dagger}_{\boldsymbol{k},1,-} c_{\boldsymbol{k}+\boldsymbol{q},2,+}] b^{\dagger}_{\boldsymbol{q}} + \mathrm{H.c.}, \tag{6}$$

where $\widetilde{E}_{k,j,\tilde{\sigma}}$ stands for the standard Rashba dispersions

$$\widetilde{E}_{j,\pm}(k) = E_j(k) \pm \alpha^R_j k = \Delta_j + \frac{\hbar^2 k^2}{2m} \pm \alpha^R_j k \tag{7}$$

shown schematically in Fig. 1(b) for the lower and upper subbands $j = 1,2$; $\Delta_1 = 0$ and $\Delta_2 = \Delta$.

The electron-photon coupling coefficients now are functions of electron momentum $\mathbf{k}$ and are spin dependent:

$$g_{++}(\boldsymbol{k},\boldsymbol{q}) = g_q e^{-i(\theta_{\boldsymbol{k}}-\theta_{\boldsymbol{k}+\boldsymbol{q}})/2} \cos\left(\frac{\theta_{\boldsymbol{k}}-\theta_{\boldsymbol{k}+\boldsymbol{q}}}{2}\right) = g_q \widetilde{g}_{++}, \tag{8}$$

$$g_{+-}(\boldsymbol{k},\boldsymbol{q}) = i g_q e^{-i(\theta_{\boldsymbol{k}}-\theta_{\boldsymbol{k}+\boldsymbol{q}})/2} \sin\left(\frac{\theta_{\boldsymbol{k}}-\theta_{\boldsymbol{k}+\boldsymbol{q}}}{2}\right) = g_q \widetilde{g}_{+-}, \tag{9}$$

$$g_{-+}(\boldsymbol{k},\boldsymbol{q}) = i g_q e^{-i(\theta_{\boldsymbol{k}}-\theta_{\boldsymbol{k}+\boldsymbol{q}})/2} \sin\left(\frac{\theta_{\boldsymbol{k}}-\theta_{\boldsymbol{k}+\boldsymbol{q}}}{2}\right) = g_q \widetilde{g}_{-+}, \tag{10}$$

$$g_{--}(\boldsymbol{k},\boldsymbol{q}) = g_q e^{-i(\theta_{\boldsymbol{k}}-\theta_{\boldsymbol{k}+\boldsymbol{q}})/2} \cos\left(\frac{\theta_{\boldsymbol{k}}-\theta_{\boldsymbol{k}+\boldsymbol{q}}}{2}\right) = g_q \widetilde{g}_{--}, \tag{11}$$

where g_q is an absolute value of the light-matter coupling coefficient defined above. The calculated matrix elements are similar to transition elements defined in Ref. 26.

Typically, the wave vector of the photon is rather small and optical transition can be treated as vertical. However, it is nonzero and its accounting can play an important role for intersubband absorption.[27] For instance, in only the Rashba case, a nonzero photon momentum $q \neq 0$ allows the spin-flip transitions ($\widetilde{g}_{+-}, \widetilde{g}_{-+} \neq 0$) and all four transitions with different energies become possible [see Fig. 1(b)]. However, the main impact for photoabsorption comes from electrons situated close to the Fermi surface, for which $q \ll k_F$. Hence, spin-flip matrix elements are proportional to the momenta ratio $\widetilde{g}_{+-}, \widetilde{g}_{-+} \sim q/k_F \ll 1$, their oscillator strength is small, and only two transitions $+ \to +$ and $- \to -$ can be expected to be visible in the experiment. Note that the energies of these transitions are different for $\alpha_1 \neq \alpha_2$, and thus they can be excited selectively by tuning the frequency of the excitation beam. In the next section, we will show that this condition leads to nonzero spin polarization generated in the system.

2. *Rashba and Dresselhaus SOI*

In the realistic QWs, the Rashba SOI is not the only interaction acting on the electron spin since due to bulk asymmetry the Dresselhaus SOI term is usually present in the Hamiltonian. The combination of both Rashba and Dresselhaus SOI leads to spin anisotropy and peculiar spin orientation in the subbands. The total electronic Hamiltonian $H = H_{\mathrm{SIA}} + H_{\mathrm{BIA}}$ [see Eqs. (1) and (2)] can be diagonalized in the same fashion as above by introduction of the operators

$$c_{\boldsymbol{k},\pm} = \frac{1}{\sqrt{2}} \left[\pm \frac{i\alpha e^{-i\theta_{\boldsymbol{k}}} + \beta e^{i\theta_{\boldsymbol{k}}}}{\sqrt{\alpha^2+\beta^2+2\alpha\beta\sin 2\theta_{\boldsymbol{k}}}} a_{\boldsymbol{k},\uparrow} + a_{\boldsymbol{k},\downarrow} \right]. \tag{12}$$

The dispersion relations for electrons are not cylindrically symmetric and have the nontrivial form

$$\widetilde{E}_j(\boldsymbol{k}) = E_j(k) \pm k\sqrt{\alpha_j^2+\beta_j^2+2\alpha\beta\sin 2\theta_{\boldsymbol{k}}}, \tag{13}$$

where j denotes the number of subbands.

In full analogy with the case when only Rashba SOI is present, one can get the matrix elements for all four optical transitions. While the calculation is straightforward, their explicit expressions are rather cumbersome and we do not present them here.

The main difference from the cases of only Rashba or Dresselhaus terms present will be the nonzero value of the coefficients g_{+-}, g_{-+} even in the limit $q \to 0$. This is because for the situation $\alpha_2, \beta_2 \neq \alpha_1, \beta_1$ spin orientation of the eigenstates corresponding to upper and lower subbands is different. The coefficients $\widetilde{g}_{+-}, \widetilde{g}_{-+}$ at zero q can be estimated as being proportional to the sine of the angle between effective magnetic fields in the upper and lower subbands, which gives $\widetilde{g}_{+-}, \widetilde{g}_{-+} \sim (\alpha_1\beta_2 - \alpha_2\beta_1)/(\alpha_1+\beta_1)(\alpha_2+\beta_2)$. In our paper, we consider the situation where this mechanism is suppressed in order to study the effect of nonzero photon momentum.

B. Spin polarization

1. *Rashba SOI*

The achievement of nonzero spin polarization is one of the main goals of spintronics. Regarding the optical generation of spin polarization (spin orientation), there are many proposals based on the interband excitation, in particular by circularly polarized light.[28] As well, there are several proposals for spin generation with intersubband transition, where optical selection rules imply that only linearly polarized light is absorbed and achieving of nonzero spin polarization becomes a formidable task. One mechanism of generation is based on the different strength of $+ \to +$ and $- \to -$ transitions due to valence band mixing, which modifies the transition matrix elements.[29] Another approach requires a different SOI effective field in both fundamental and excited subbands, leading to overall nonzero spin polarization.[30] Here we want to study the possibility of spin polarization generation which is linearly proportional to the photon wave vector q.

The average spin of the electron in the second quantization representation reads as[31,32]

$$\langle \hat{S} \rangle = \sum_{k\sigma\sigma'} \langle k\sigma' | \hat{S} | k\sigma \rangle c^{\dagger}_{k,\sigma'} c_{k,\sigma}, \tag{14}$$

where we defined the spin operator $\hat{S} = \frac{\hbar}{2}(\sigma_x, \sigma_y, \sigma_z)$ with σ_i being Pauli matrices given for each direction ($i = x, y, z$). It is

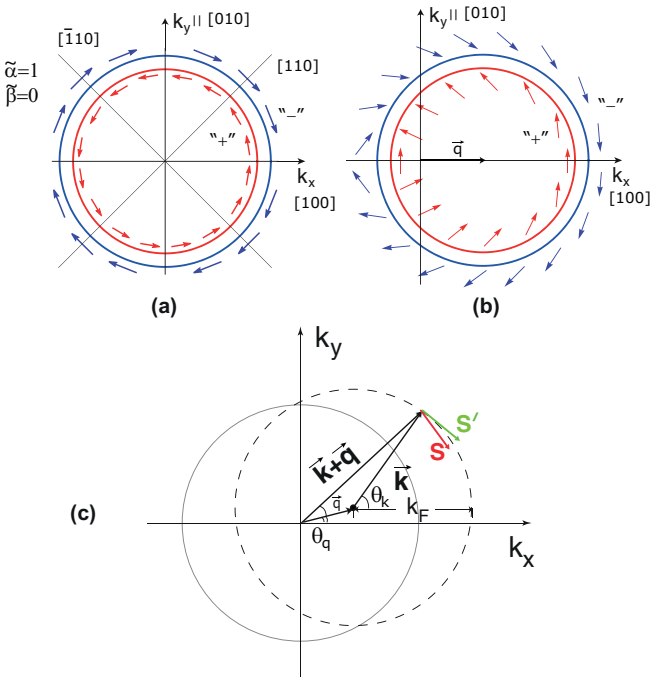

FIG. 2. (Color online) (a) Orientation of electron spin in + and − Rashba split subbands without accounting of photon momentum ($q = 0$). (b) Vector plot of spin orientation with accounting of finite photon momentum ($q/k_F = 0.3$, $\theta_q = 0$). (c) Schematic representation of nonzero photon momentum q influence on spin polarization.

reminiscent to the first quantization definition of average spin given as $S_{k,\pm} = \langle \Psi_{k,\pm} | \hat{\sigma} | \Psi_{k,\pm} \rangle$.[33]

First, let us consider the case of fully thermalized electron gas and calculate the average spin within the subband. The average spin projection onto x and y directions for the case of the Rashba SOI is given by

$$\langle +|S_x|+\rangle = \sum_{\mathbf{k}} \sin\theta_k = \int_0^{k_+} \frac{k\,dk}{(2\pi)^2} \int_0^{2\pi} d\theta_k \sin\theta_k, \quad (15)$$

$$\langle +|S_y|+\rangle = \sum_{\mathbf{k}} (-\cos\theta_k) = \int_0^{k_+} \frac{k\,dk}{(2\pi)^2} \int_0^{2\pi} d\theta_k (-\cos\theta_k), \quad (16)$$

$$\langle -|S_x|-\rangle = \sum_{\mathbf{k}} (-\sin\theta_k) = \int_0^{k_-} \frac{k\,dk}{(2\pi)^2} \int_0^{2\pi} d\theta_k (-\sin\theta_k), \quad (17)$$

$$\langle -|S_y|-\rangle = \sum_{\mathbf{k}} \cos\theta_k = \int_0^{k_-} \frac{k\,dk}{(2\pi)^2} \int_0^{2\pi} d\theta_k \cos\theta_k, \quad (18)$$

and one can see the orientation for spin in ++ and −− transitions given by vectors $\mathbf{S}_+ = (\sin\theta_k, -\cos\theta_k, 0)$ and $\mathbf{S}_- = (-\sin\theta_k, \cos\theta_k, 0)$ with three spatial components $\mathbf{S} = (S_x, S_y, S_z)$. The modified radii of the Fermi surface for + and − spin subbands are written as $k_\pm = k_F(1 \mp \eta_R)$ [see Fig. 1(b)], where $\eta_R = \alpha m/\hbar^2 k_F$. The electron spin orientation for spin subbands is shown in Fig. 2(a). Obviously, the integration over angle θ_k yields zero average spin projections $\langle \pm|S_{x,y}|\pm\rangle = 0$.

Now, let us consider the situation when electrons are constantly optically excited to the upper subband due to cavity photon absorption. The spin of an electron in the presence of spin-orbital interaction of Rashba type is perpendicular to its momentum direction. Therefore, with accounting of finite wave vector of the photon, one can see that the spin state in Fig. 2(c) is no longer given by vector $\mathbf{S}'$, but by $\mathbf{S}$. This corresponds to the change of spin states to $\mathbf{S}_+ = (\sin\theta_{k+q}, -\cos\theta_{k+q}, 0)$ and $\mathbf{S}_- = (-\sin\theta_{k+q}, \cos\theta_{k+q}, 0)$. Now, the boundaries of integration are changed due to the shift of Fermi circles and for selective excitation of ++ and −− transitions are given by the expression

$$k'_\pm = k_\pm \left[\sqrt{1 - \frac{q^2}{k_\pm^2} \sin^2(\theta_k - \theta_q)} + \frac{q\cos(\theta_k - \theta_q)}{k_\pm} \right]. \quad (19)$$

The average spin projections with accounting of photon momentum can be rewritten using the relations

$$\cos\theta_{k+q} = \frac{k\cos\theta_k + q\cos\theta_q}{\sqrt{k^2 + q^2 + 2kq\cos(\theta_k - \theta_q)}}, \quad (20)$$

$$\sin\theta_{k+q} = \frac{k\sin\theta_k + q\sin\theta_q}{\sqrt{k^2 + q^2 + 2kq\cos(\theta_k - \theta_q)}}, \quad (21)$$

where θ_q denotes the angle between vector $\mathbf{q}$ and the x axis, and all variables are shown explicitly on the sketch in Fig. 2(c). One should keep in mind that the Fermi circle for $q \neq 0$ is θ_k dependent. Therefore, it requires advanced momentum integration with consequent angular integration and can be done only numerically. To obtain the dimensionless quantity connected to the average spin of electron gas (or spin polarization), one should normalize the result of integration dividing it by the population in each subband $n_\pm = k_\pm^2/4\pi$.

One sees that while for the $q = 0$ case the average spin is zero, the accounting of Fermi circle shift gives preferable direction to the spin of excited electrons, which is [010] for the $\theta_q = 0$ incident angle shown in Fig. 2(b). This effect is similar to the spin-galvanic effect observed previously for the interband case and connected to the nonzero charge current.[19,34]

We remind that for achievement of nonzero spin polarization, the constants of Rashba SOI have to be different in the first and second subbands of QW. This condition ensures that ++ and −− transitions occur at different rates, or equivalently energies of ++ and −− transitions are different. This condition is usually realized experimentally for GaAs samples.

2. *Rashba and Dresselhaus SOI*

Following the scheme used in the previous section for the spin-isotropic Rashba splitting, we derive the same quantities for the spin-anisotropic case of the combined Rashba and Dresselhaus interaction.

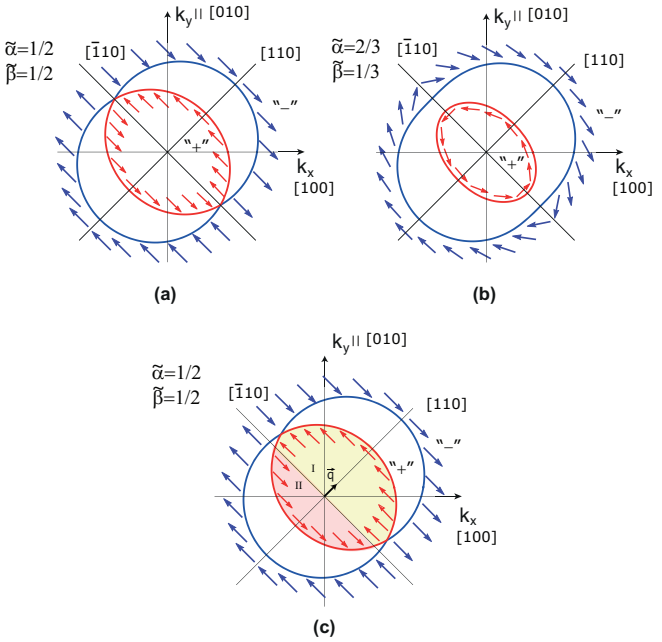

FIG. 3. (Color online) Orientation of electron spin in + and − Rashba and Dresselhaus split subbands for equal SOI strength (a) and for the $\tilde{\alpha}=\frac{2}{3}$, $\tilde{\beta}=\frac{1}{3}$ case (b). (c) The spin vector plot for equal Rashba and Dresselhaus SOI with accounting of finite photon momentum, which leads to the Fermi surface shift in the [110] direction. The areas I (yellow filled) and II (pink filled) show the difference in spin orientation.

The spin orientation can be found using the spin states for the Rashba and Dresselhaus case (12) and is given by

$$\langle +|S_x|+\rangle = \sum_{\mathbf{k}} \frac{\tilde{\alpha}\sin\theta_k + \tilde{\beta}\cos\theta_k}{\sqrt{\tilde{\alpha}^2+\tilde{\beta}^2+2\tilde{\alpha}\tilde{\beta}\sin 2\theta_k}}, \quad (22)$$

$$\langle +|S_y|+\rangle = \sum_{\mathbf{k}} \frac{-\tilde{\alpha}\cos\theta_k - \tilde{\beta}\sin\theta_k}{\sqrt{\tilde{\alpha}^2+\tilde{\beta}^2+2\tilde{\alpha}\tilde{\beta}\sin 2\theta_k}}, \quad (23)$$

$$\langle -|S_x|-\rangle = \sum_{\mathbf{k}} \frac{-\tilde{\alpha}\sin\theta_k - \tilde{\beta}\cos\theta_k}{\sqrt{\tilde{\alpha}^2+\tilde{\beta}^2+2\tilde{\alpha}\tilde{\beta}\sin 2\theta_k}}, \quad (24)$$

$$\langle -|S_y|-\rangle = \sum_{\mathbf{k}} \frac{\tilde{\alpha}\cos\theta_k + \tilde{\beta}\sin\theta_k}{\sqrt{\tilde{\alpha}^2+\tilde{\beta}^2+2\tilde{\alpha}\tilde{\beta}\sin 2\theta_k}}, \quad (25)$$

where we defined dimensionless Rashba and Dresselhaus constants $\tilde{\alpha}=\alpha/(\alpha+\beta)$ and $\tilde{\beta}=\beta/(\alpha+\beta)$, respectively. The vector plot of spin orientation for different Rashba and Dresselhaus constants is shown in Figs. 3(a) and 3(b). One sees that while for $\tilde{\alpha}=\frac{2}{3}$, $\tilde{\beta}=\frac{1}{3}$ the spin pattern is close to the Rashba case, but with preferred directions being $[\bar{1}10]$ and $[1\bar{1}0]$, for equal Rashba and Dresselhaus SOI strength ($\tilde{\alpha}=\tilde{\beta}=\frac{1}{2}$) the spin orientation approaches a steplike function which changes sign in $\theta_k=3\pi/4$ and $7\pi/4$ points. The Fermi surfaces for upper (+) and lower (−) spin subbands now are given by the expression $k_\pm = k_F[1\mp\eta(\theta_k)]$ with $\eta(\theta_k)=\frac{m}{\hbar^2 k_F}\sqrt{\alpha^2+\beta^2+2\alpha\beta\sin 2\theta_k}$.

Accounting for the nonzero photon momentum results into the change of spin states $\mathbf{S}(\theta_\mathbf{k}) \to \mathbf{S}'(\theta_{\mathbf{k}+\mathbf{q}})$. Additionally, one should account for angle-dependent shifted Fermi surfaces

$$k'_\pm = k'_\pm\left[\sqrt{1-\frac{q^2}{k'^2_\pm}\sin^2(\theta_k-\theta_q)}+\frac{q\cos(\theta_k-\theta_q)}{k'_\pm}\right], \quad (26)$$

where shifted Fermi circles are angle dependent, $k'_\pm = 1\mp\eta(\Theta_{k,q})$ with $\eta(\Theta_{k,q})=\frac{m}{\hbar^2 k_F}\sqrt{\alpha^2+\beta^2+2\alpha\beta\sin 2\Theta_{k,q}}$ and $\Theta_{k,q}=\arctan[\frac{k\sin\theta_k - q\sin\theta_q}{k\cos\theta_k - q\cos\theta_q}]$. Similarly to the isotropic Rashba case, for $q=0$ the average spin vanishes, while for finite photon wave vector q, the net spin is not equal to zero. The effect is most clear for equal Rashba and Dresselhaus SOI. Then, the average spin can be seen as the difference of areas I and II in Fig. 3(c). Moreover, one can note that the $\tilde{\alpha}=\tilde{\beta}=\frac{1}{2}$ case is strongly anisotropic regarding the photon incidence direction θ_q [Figs. 4(a) and 4(b)]. While for $\theta_q=\pi/4$ it has a maximum absolute value, spin polarization does not appear in the system for the $\theta_q=3\pi/4$ angle of incidence. The average spin vector $\langle\vec{S}\rangle$ is oriented perpendicular to $\mathbf{q}$.

We calculate the dependence of spin polarization on the orientation of an incident light angle θ_q. The corresponding

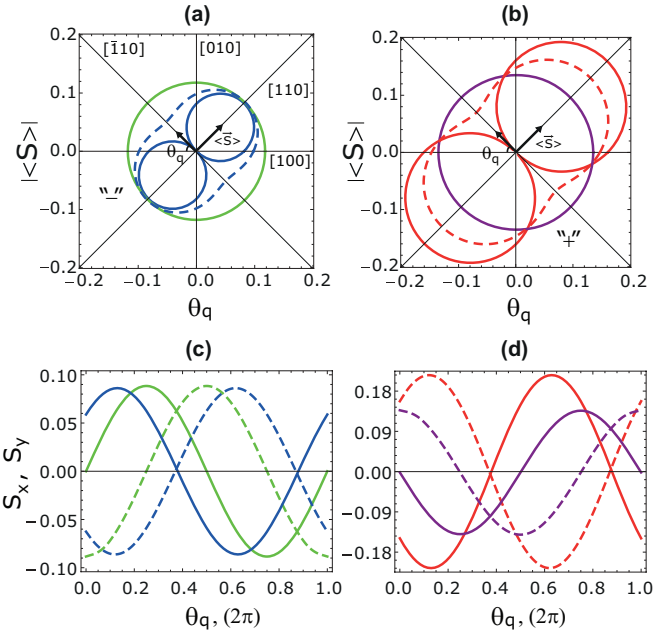

FIG. 4. (Color online) (a) and (b) Polar plots of absolute value of an average spin vector as a function of photon incident angle θ_q for $--$ (a) and $++$ (b) transitions. (a) Green solid circle corresponds to the Rashba SOI only case ($\tilde{\alpha}=1,\tilde{\beta}=0$). Blue solid circles show strong anisotropic dependence of spin polarization on the incident angle θ_q for equal Rashba and Dresselhaus strength ($\tilde{\alpha}=\tilde{\beta}=\frac{1}{2}$). The blue dashed line shows transient behavior for the $\tilde{\alpha}=\frac{2}{3}$ and $\tilde{\beta}=\frac{1}{3}$ case. (b) Purple solid circle corresponds to the isotopic Rashba SOI case ($\tilde{\alpha}=1,\tilde{\beta}=0$). Red solid circles show spin polarization as a function of incident angle θ_q for equal Rashba and Dresselhaus strength ($\tilde{\alpha}=\tilde{\beta}=\frac{1}{2}$). The red dashed line shows transient behavior for the $\tilde{\alpha}=\frac{2}{3}$ and $\tilde{\beta}=\frac{1}{3}$ case. (c) and (d) Spin-polarization projections on the x (solid lines) and y (dashed lines) axis as a function of photon incident angle θ_q for $--$ (c) and $++$ (d) transitions. Green and purple lines correspond to only the Rashba case; blue and red lines correspond to equal Rashba and Dresselhaus SOI. All dependencies are calculated for $q/k_F=0.06$.

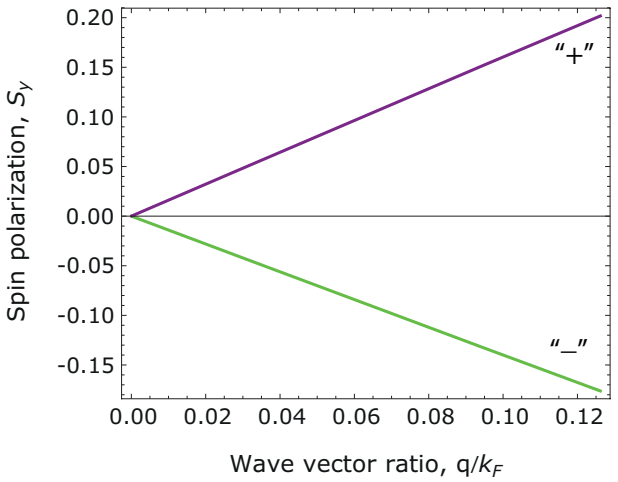

FIG. 5. (Color online) Spin polarization as a function of wave vector ratio q/k_F for the Rashba case plotted for $+$ and $-$ subbands (purple and green solid lines). Here we fixed incidence angle $\theta_q = 0$ and show S_y component of polarization.

polar plots are represented in Figs. 4(a) and 4(b) for selective excitation of $--$ (a, green solid circle) and $++$ (b, purple solid circle) transitions. Note that in the case where only the Rashba term is present, the absolute value of average spin is the same for all θ_q. The orientation of average spin vector is defined by the θ_q angle and is aligned perpendicular to the vector $\mathbf{q}$ (Fig. 4, $\langle\vec{S}\rangle$ label on the plot). In the case of equal Rashba and Dresselhaus SOI, the strong anisotropy of the polar pattern is observed (blue and red solid line). Dashed lines in Figs. 4(a) and 4(b) correspond to not equal Rashba and Dresselhaus SOI and depict the transient regime between the spin-anisotropic to spin-isotropic case. Additionally, in Figs. 4(c) and 4(d), we show the same dependencies for the x and y projections of spin polarization.

Furthermore, we study the dependence of spin polarization on the wave-vector ratio q/k_F which defines the relative value of the Fermi circle shift under optical excitation. Since the photon wave-vector value usually does not overcome inverse micrometer $q < 10^6$ m^{-1}, the experimental way to tune the q/k_F ratio relies on changing the carrier density. The plot of net spin polarization as a function of momenta ratio q/k_F is given in Fig. 5 for $--$ and $++$ transitions (green and purple solid lines). Higher values of spin polarization for lower spin subband come from the fact that $k_- < k_F < k_+$. One can see the linear dependence for the case of isotropic SOI for the realistic values of the wave-vector ratio. The behavior of average spin on the large scale shows saturation for region where the photon wave vector approaches the value of Fermi circle radius with spin polarization approaching unity. However, first, this situation does not have substantial physical background since for small concentrations ($q \approx k_F \approx 10^6$ m^{-1}) even small excitation leads to the strongly nonequilibrium situation and this situation can not be treated within our approach. Second, the visible separation of polaritonic modes implies that separation between bare transition modes $\epsilon_s = 2(\alpha_2 - \alpha_1)k_F$ is greater than photon decay rate ($\Gamma \approx 0.5$ meV), which puts the lower boundary for the k_F value. Finally, for the ratio q/k_F closer to unity, one should account for $+-$ and $-+$ transitions on the same footing with $++$ and $--$ transitions, and we do not consider this situation.

C. Spin currents

In the following section, we briefly discuss the possibility of spin-current generation by intersubband optical excitation. The concept of spin currents lies in the origin of spintronics since it allows us to design devices based on manipulation of spin degree of freedom of the carriers. However, effective creation of spin currents is not a trivial task. The proposed schemes include injection from ferromagnetic leads to semiconductor,[12] creation of nonequilibrium distribution of carriers by applying voltage[19] or by optical excitation[26,35,36] in structures with spin-orbit interaction. The photocurrents associated with nonzero spin polarization were studied in the context of interband transition with spin-split bands shined by circularly polarized light.[37–39] The inverse effect, namely, the appearance of charge current due to nonequilibrium population of electron spins, was observed by Ganichev *et al.*[34] and named the spin-galvanic effect. The review on the subject can be found in Ref. 40.

In the system with spin-split upper and lower subbands, the intersubband transitions occur with spin conservation. Due to the difference in the SOI constants for the upper and lower subbands, the $++$ and $--$ transitions have different energies. An absorption of TM polarized photon leads to the electron in the upper subband with momentum k (first we consider vertical transition) and "hole" in the lower subband with the opposite momentum (see Fig. 6). Moreover, we account for the Rashba SOI with peculiar spin orientation in the spin subbands. The excitation of carriers on the Fermi disk leads to the generation of spin and charge currents (Fig. 6, top). However, for the case of vertical transition, charge current is zero and the situation corresponds to the generation of *pure* spin currents. The expression for the pure spin current in the

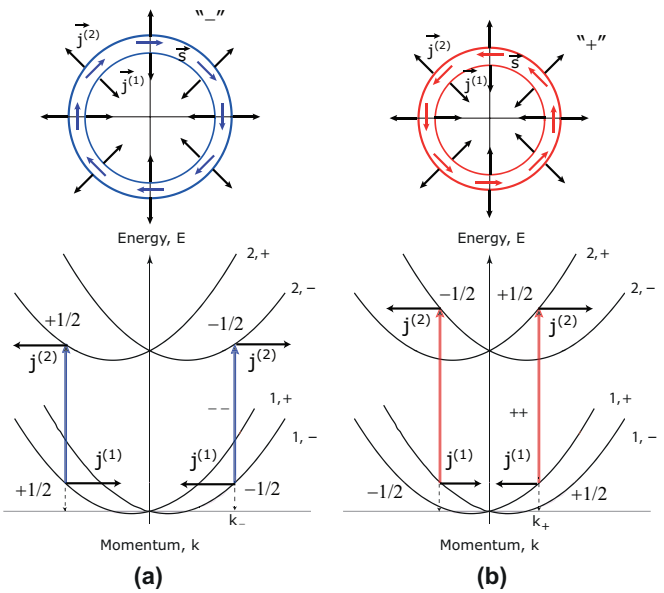

FIG. 6. (Color online) Sketch of spin-current orientation ($\vec{j}$, black arrows) for the $--$ (a) and $++$ (b) transitions. The colored lines show the spin orientation of electrons ($\vec{s}$).

general form can be described by the pseudotensor $\widehat{\mathbf{J}}$ with components[35]

$$J_{\mu}^{\nu} = \sum_{k} \tau_e \mathrm{Tr}\left[\frac{\sigma_\mu}{2}\mathbf{v}_\nu \rho(\mathbf{k})\right], \tag{27}$$

where $\mathbf{v}(\mathbf{k})$ is velocity operator, $\rho(\mathbf{k})$ is the spin density matrix, and τ_e is relaxation time. This formula applied to the intersubband transition describes the spin currents in the ν direction with spin aligned in the μ direction. One should note that it is valid only in the first order of spin-orbit coupling. However, strictly speaking, Pauli matrices do not commute with velocity operator, and one should take the symmetrized product of these operators.[26]

In the previous section we have shown that accounting for the finite photon momentum leads to the nonzero average spin of intersubband excitation. Thus, it creates a nonequilibrium situation similar to the electric field displacement of Fermi disks,[19] when the charge current in the system does not vanish and spin current with spin polarization defined by incident angle θ_q is generated. While we do not derive the expressions for spin current in the $q \neq 0$ case, the behavior can be qualitatively understood in connection with previous section.

Finally, the implementation of strong-coupling between photonic mode and intersubband excitation affects the spin currents. Due to coherence of cavity mode, the resulted spin currents will have the long coherence length and can be used for spinoptronic applications.[41]

III. INTERSUBBAND POLARITONS WITH SOI

A. Elementary excitation spectrum

In the case when the QW is placed inside a microcavity which is tuned in resonance with intersubband transition, the photons can undergo multiple reemissions and reabsorptions and hybrid intersubband polariton modes can be formed.[8,9] The powerful theoretical tool for their description is a many-body diagrammatic technique.[10] The quantities which define the physical properties of the system are the photon Green's function and polarization operator, shown diagrammatically in Figs. 7(a) and 7(b), respectively. The poles of the renormalized photon Green's function give the spectrum of elementary excitations in the system, while the imaginary part of the polarization operator allows us to calculate the absorption spectrum.

If one neglects the electron-electron interactions, the polarization operators corresponding for four possible types of transitions in the system $(++, --, +-, -+)$ read as

$$\Pi_0^{\widetilde{\sigma}\widetilde{\sigma}'}(\omega,q) = \int \frac{d\boldsymbol{k}}{(2\pi)^2} \frac{\left|\widetilde{g}^2_{\widetilde{\sigma}\widetilde{\sigma}'}(q,\varphi)\right|}{\hbar\omega + E_{\boldsymbol{k},1,\widetilde{\sigma}} - E_{\boldsymbol{k}+\boldsymbol{q},2,\widetilde{\sigma}'} + i\gamma}, \tag{28}$$

where we defined $\varphi = \theta_{\boldsymbol{k}} - \theta_{\boldsymbol{k}+\boldsymbol{q}}$ and $\widetilde{\sigma},\widetilde{\sigma}' = \pm$ denote different spin subbands ($+$ and $-$). The energy of the electron in the fundamental subband is $E_{1,\widetilde{\sigma}}(\boldsymbol{k}) = \hbar^2k^2/2m \pm \alpha_1 k$ and in the upper subband is $E_{2,\widetilde{\sigma}}(\boldsymbol{k}+\boldsymbol{q}) = \Delta + \hbar^2(\boldsymbol{k}+\boldsymbol{q})^2/2m \pm \alpha_2|\boldsymbol{k}+\boldsymbol{q}|$. Dimensionless coefficients $\widetilde{g}_{\widetilde{\sigma}\widetilde{\sigma}'}(q,\varphi)$ are defined

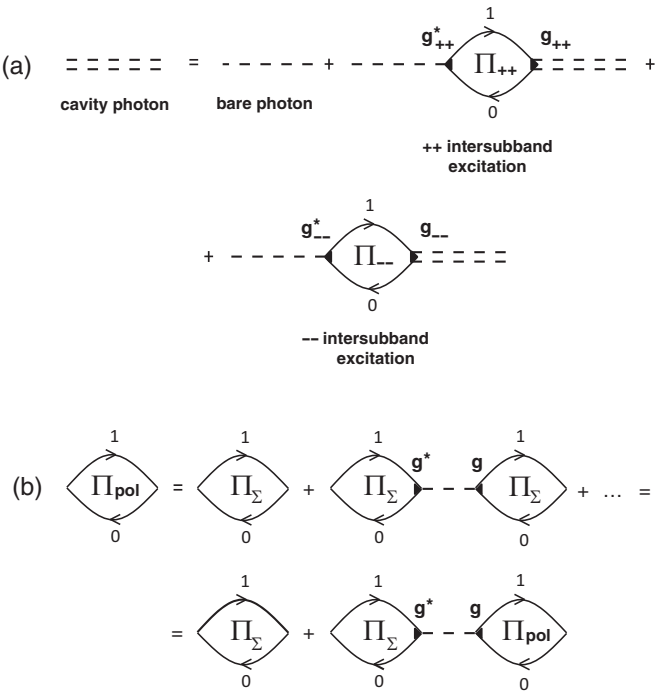

FIG. 7. Diagrammatic representation of intersubband polaritons. (a) The Dyson equation for the Green's function of the microcavity photon interacting with $++$ and $--$ intersubband transitions $\Pi_{\pm,\pm}$. $g_\pm$ corresponds to the interaction constant, indices 1 and 0 denote the excited and fundamental subbands, respectively. (b) Dyson equation for polarization operators governing the absorbtion spectrum of intersubband quasiparticles coupled to the cavity mode where $\Pi_\Sigma = \Pi_{++} + \Pi_{--}$.

by Eqs. (8)–(11) and read as

$$\begin{aligned} |\widetilde{g}^2_{++}(q,\varphi)| &= |\widetilde{g}^2_{--}(q,\varphi)| = \cos^2\varphi/2 = \tfrac{1}{2}(1+\cos\varphi), \\ |\widetilde{g}^2_{+-}(q,\varphi)| &= |\widetilde{g}^2_{-+}(q,\varphi)| = \sin^2\varphi/2 = \tfrac{1}{2}(1-\cos\varphi). \end{aligned} \tag{29}$$

It was already mentioned in Sec. II A that while $|\widetilde{g}^2_{\pm\pm}|$ interaction constants corresponding to $++,--$ transitions are close to unity, the $+-,-+$ transitions do not play a substantial role. The quantitative estimate can be done using realistic values of electron concentration with Fermi momentum of the order $k_F \approx 10^8$ m^{-1} ($n = 10^{11}$ cm^{-2}) and microcavity photon momentum q in the point of anticrossing $q = 10^6$ m^{-1} for negative detuning $\delta = -5$ meV. The angle is typically small $\varphi = \theta_k - \theta_{k+q} \approx \arcsin(q/k_F) \approx 10^{-2}$, which reduces the oscillator strength of spin-flip transitions $\widetilde{g}^2_{\widetilde{\sigma}\widetilde{\sigma}'}(q,\varphi)$ by five orders of magnitude. Consequently, they give minor contribution in the case of strong light-matter coupling, and we omit them in the Dyson equation for the cavity photon Green's function shown in Fig. 7(a). The polarization operators corresponding to $++$ and $--$ transitions can be calculated by performing analytical integration on angle in (28) with subsequent numerical integration on absolute value of wave vector k.

The dispersion of elementary particles in the system is defined by the poles of renormalized photon Green's function $D(q,\omega)$, which can be found by solving the Dyson equation,

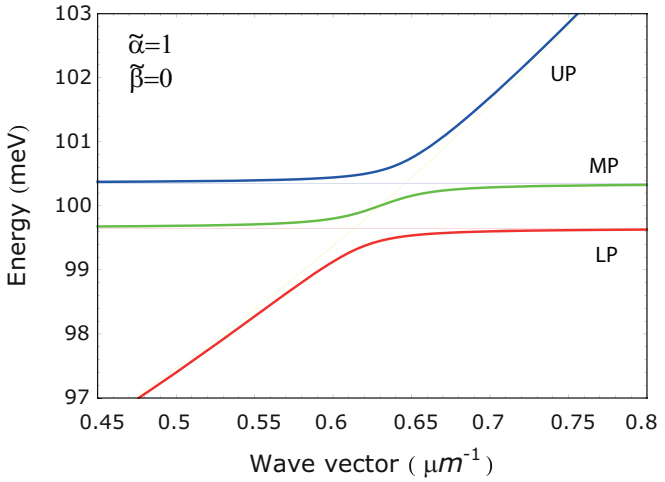

FIG. 8. (Color online) Dispersions of intersubband polariton modes with accounting of isotropic Rashba splitting. The red line corresponds to the lower polariton (LP) and coincides with $--$ excitation dispersion for large momenta, while the blue line shows the upper polariton (UP) which is reminiscent to $++$ excitation for small wave vectors. The green line describes the middle or mixed polariton (MP), being a transitional branch between the lower and upper polaritonic branches.

and reads as

$$D = \frac{D_0}{1 - g_q^2(\Pi_{++} + \Pi_{--})D_0}, \tag{30}$$

where $\Pi_{\pm,\pm}$ are polarization operators described before, q_q is given by Eq. (4), and D_0 is a bare photon Green's function

$$D_0(\omega,q) = \frac{2\hbar\omega_0(q)}{\hbar^2\omega^2 - \hbar^2\omega_0^2(q) + 2i\Gamma\omega_0(q)}, \tag{31}$$

where $\omega_0(q)$ denotes cavity mode dispersion and Γ is a broadening of photonic mode due to the finite lifetime of the cavity photon (taken to be $\approx$10 ps). The explicit expression for the electron-photon interaction matrix element g_q is given by Eq. (4).

The spectrum of the elementary excitations of intersubband transitions coupled to the cavity mode with accounting of Rashba SOI is plotted in Fig. 8(a). Here, we considered AQW of $L = 12.8$ nm width with frequency of bare transition equal to $\Delta = 100$ meV at $k = 0$ point and concentration of electron gas $n = 10^{11}$ cm^{-2}. The Rashba constants for the lower and upper subbands were taken to be $\alpha_1 = 0.9$ meV nm and $\alpha_2 = 6$ meV nm, respectively,[26] and we neglected Dresselhaus terms for simplicity. Both $++$ and $--$ spin-dependent transitions are in the strong-coupling regime with the cavity mode. As transition frequencies are different, one observes the formation of three polariton branches. This differs from the usually considered spin-independent case for which only two polaritonic branches exist. Intersubband polariton modes can be selectively excited by the resonant excitation of a given frequency. As it was discussed above, such excitation will induce spin currents in the system.

While the consideration of simultaneous Rashba and Dresselhaus interaction can be done in the same fashion, it does not lead to qualitative differences compared to the isotropic Rashba case and we do not address this point here.

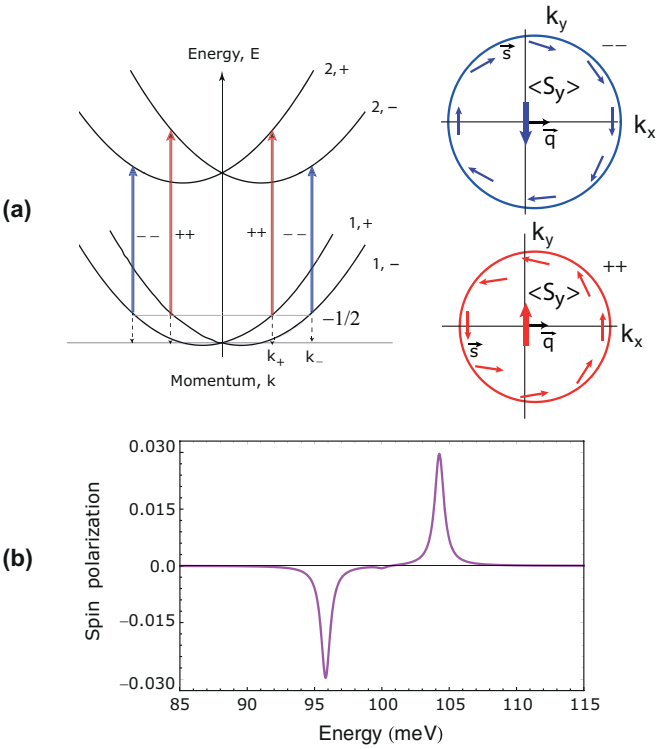

FIG. 9. (Color online) (a) Sketch of the spin-polarization spectral behavior of intersubband excitations. (b) The spin-polarization degree as a function of pumping laser energy for the photon wave vector $q = 6.25$ μm^{-1}. Changing the laser frequency allows one to excite selectively upper, middle, or lower polariton modes. This results into a change of the net spin polarization.

The energy splitting between $++$ and $--$ transitions is approximately equal to $\epsilon_s = 2(\alpha_2 - \alpha_1)k_F$. For instance, with the given parameters α_2 and α_1 and for concentration $n = 10^{11}$ cm^{-2}, it has the value $\epsilon_s = 0.8$ meV, which is already comparable to the broadening of the photonic mode. Therefore, for the experimental observation of the effect, one should search for the sample with large difference in Rashba constants, and InAs-based QWs are promising candidates for this purpose.

In the present calculations, we did not account for electron-electron interactions. However, it was shown that under certain conditions, they can play a substantial role.[10] Namely, in the case of doped quantum well where concentration of electron exceeds $n = 10^{12}$ cm^{-2}, the elementary excitations are the intersubband plasmon polaritons, and not single-particle excitations. This in principle can lead to modification of the spin-polarization properties of the modes. However, in order to keep the effect as large as possible, one should make large q/k_F, and therefore choose the sample with comparably small electron density ($n \approx 10^{11}$ cm^{-2}). In this case, plasmonic corrections play a minor role.

Next, we calculate the net spin polarization as a function of excitation frequency. The system can be described by the three coupled oscillators model, where $++$ and $--$ intersubband excitations are coupled to the cavity photon. The Hamiltonian of the system can be diagonalized using Hopfield transformations, with squares of Hopfield coefficients giving the fraction of bare mode in the polariton state.[42] The $++$

and $--$ intersubband excitations are associated with nonzero spin polarization in the system. For instance, we can fix the pumping angle to $\theta_q = 0$, and the resulting net spin lies in the y direction [Fig. 9(a)]. Moreover, spin polarizations for $++$ and $--$ will have opposite sign. The total spin polarization of intersubband polaritons thus reads as[28]

$$P_k^i = \frac{|C_{++}^i|^2 - |C_{--}^i|^2}{|C_{++}^i|^2 + |C_{--}^i|^2}, \tag{32}$$

where $P^i(k)$ is spin polarization of the ith mode and $|C_{++}^i|^2$ means the fraction of $++$ excitation in the $i = L,M,U$ lower, middle, and upper polaritonic modes. The spectral dependence of spin polarization can be calculated using the simple expression

$$P_{\text{tot}}(\omega) = \sum_{i=L,M,U} P_k^i \, \text{Im}\Pi_i(\omega), \tag{33}$$

where $\text{Im}\Pi_i(\omega)$ represents the spectral dependence of decomposed absorption peaks for each polaritonic branch. The resulted plot is shown in Fig. 9(b). Here, we fixed incident light vector to anticrossing point. Consequently, by tuning the frequency of the pumping laser, one can manipulate with total spin polarization in the system.

Due to the coupling with the photonic mode, spin currents induced in the coupled QW-microcavity system will have a much bigger decoherence length compared to the electron currents.[43] This makes the considered system a promising candidate for spintronic and spinoptronic applications.

IV. CONCLUSIONS

In conclusion, we analyzed the optical properties of the spin-dependent intersubband transition in asymmetric quantum wells. We have shown that accounting of finite photon momentum leads to the optical orientation effect. We also calculated the spectrum of elementary excitations arising from strong coupling of the photonic mode with an intersubband transition of an asymmetric QW. The calculated spectrum of elementary excitations shows the appearance of upper, lower, and middle polaritonic modes. The possibility of the generation of spin currents with long coherence lengths is discussed.

ACKNOWLEDGMENTS

We would like to thank M. M. Glazov and S. A. Tarasenko for useful discussions and the critical reading of the manuscript. This work was supported by Rannis "Center of Excellence in Polaritonics" and FP7 IRSES project "SPINMET". O.K. acknowledges the support from Eimskip Fund.

[1] E. Dupont, H. C. Liu, A. J. SpringThorpe, W. Lai, and M. Extavour, Phys. Rev. B **68**, 245320 (2003).
[2] C. Walther, M. Fischer, G. Scalari, R. Terazzi, N. Hoyler, and J. Faist, Appl. Phys. Lett. **91**, 131122 (2007).
[3] O. Cathabard, R. Teissier, J. Devenson, J. C. Moreno, and A. N. Baranov, Appl. Phys. Lett. **96**, 141110 (2010).
[4] D. Oustinov, N. Jukam, R. Rungsawang, J. Madeo, S. Barbieri, P. Filloux, C. Sirtori, X. Marcadet, J. Tignon, and S. Dhillon, Nat. Commun. **1**, 69 (2010).
[5] J. Faist, F. Capasso, D. L. Sivco, C. Sirtori, A. L. Hutchinson, and A. Y. Cho, Science **264**, 553 (1994).
[6] R. Colombelli, C. Ciuti, Y. Chassagneux, and C. Sirtori, Semicond. Sci. Technol. **20**, 985 (2005).
[7] *Intersubband Transitions in Quantum Wells: Physics and Device Applications I*, edited by H. C. Liu and F. Capasso, Semiconductors and Semimetals (Academic, San Diego, 2000), Vol. 62.
[8] D. Dini, R. Kohler, A. Tredicucci, G. Biasiol, and L. Sorba, Phys. Rev. Lett. **90**, 116401 (2003).
[9] M. Geiser, F. Castellano, G. Scalari, M. Beck, L. Nevou, and J. Faist, Phys. Rev. Lett. **108**, 106402 (2012).
[10] O. Kyriienko and I. A. Shelykh, J. Nanophotonics **6**, 061804 (2012).
[11] S. A. Wolf, D. D. Awschalom, R. A. Buhrman, J. M. Daughton, S. von Molnar, M. L. Roukes, A. Y. Chtchelkanova, and D. M. Treger, Science **294**, 1488 (2001).
[12] I. Zutic, J. Fabian, and S. Das Sarma, Rev. Mod. Phys. **76**, 323 (2004).
[13] S. Datta and B. Das, Appl. Phys. Lett. **56**, 665 (1990).
[14] I. A. Shelykh, A. V. Kavokin, Yu. G. Rubo, T. C. H. Liew, and G. Malpuech, Semicond. Sci. Technol. **25**, 013001 (2010).
[15] I. A. Shelykh, K. V. Kavokin, A. V. Kavokin, G. Malpuech, P. Bigenwald, H. Deng, G. Weihs, and Y. Yamamoto, Phys. Rev. B **70**, 035320 (2004).
[16] I. A. Shelykh, G. Pavlovic, D. D. Solnyshkov, and G. Malpuech, Phys. Rev. Lett. **102**, 046407 (2009).
[17] T. C. H. Liew, I. A. Shelykh, and G. Malpuech, Phys. E (Amsterdam) **43**, 1543 (2011).
[18] R. Winkler, *Spin-Orbit Coupling Effects in Two-Dimensional Electron and Hole Systems*, Springer Tracts in Modern Physics (Springer, Berlin, 2003), Vol. 191.
[19] R. H. Silsbee, J. Phys.: Condens. Matter **16**, R179 (2004).
[20] Yu. A. Bychkov and E. I. Rashba, Pis. Zh. Eksp. Teor. Fiz. **39**, 66 (1984) [Sov. Phys.–JETP **39**, 78 (1984)] .
[21] J. Nitta, T. Akazaki, H. Takayanagi, and T. Enoki, Phys. Rev. Lett. **78**, 1335 (1997).
[22] J. P. Heida, B. J. van Wees, J. J. Kuipers, T. M. Klapwijk, and G. Borghs, Phys. Rev. B **57**, 11911 (1998).
[23] G. Engels, J. Lange, Th. Schapers, and H. Luth, Phys. Rev. B **55**, 1958 (1997).
[24] E. A. de Andrada e Silva, G. C. La Rocca, and F. Bassani, Phys. Rev. B **55**, 16293 (1997).
[25] G. Dresselhaus, Phys. Rev. **100**, 580 (1955).
[26] E. Ya. Sherman, A. Najmaie, and J. E. Sipe, Appl. Phys. Lett. **86**, 122103 (2005).
[27] L. E. Golub, Europhys. Lett. **98**, 54005 (2012).
[28] F. Meier and B. P. Zakharchenya, *Optical Orientation* (North-Holland, New York, 1984).
[29] E. L. Ivchenko and S. A. Tarasenko, J. Exp. Theor. Phys. **99**, 379 (2004).

[30]S. A. Tarasenko, Phys. Solid State **49**, 1787 (2007).
[31]H. Bruus and K. Flensberg, *Many Body Quantum Theory in Condensed Matter Physics* (Oxford University Press, New York, 2004).
[32]G. D. Mahan, *Many Particles Physics* (Plenum, New York, 1993).
[33]N. S. Averkiev and M. M. Glazov, Semiconductors **42**, 958 (2008).
[34]S. D. Ganichev, E. L. Ivchenko, V. V. Belakov, S. A. Tarasenko, M. Sollinger, D. Weiss, W. Wegscheider, and W. Prettl, Nature (London) **417**, 153 (2002).
[35]E. L. Ivchenko and S. A. Tarasenko, Semicond. Sci. Technol. **23**, 114007 (2008).
[36]S. A. Tarasenko and E. L. Ivchenko, JETP Lett. **81**, 231 (2005).
[37]E. L. Ivchenko, Y. B. Lyanda-Geller, and G. E. Pikus, Pis. Zh. Eksp. Teor. Fiz. **50**, 156 (1989) [Sov. Phys.–JETP Lett. **50**, 175 (1989)].
[38]E. L. Ivchenko, Y. B. Lyanda-Geller, and G. E. Pikus, Zh. Eksp. Teor. Fiz. **98**, 989 (1990) [Sov. Phys.–JETP **71**, 550 (1990)].
[39]R. D. R. Bhat and J. E. Sipe, Phys. Rev. Lett. **85**, 5432 (2000).
[40]S. D. Ganichev and W. Prettl, J. Phys.: Condens. Matter **15**, R935 (2003).
[41]M. M. Glazov, Solid State Commun. **142**, 531 (2007).
[42]H. Deng, H. Haug, and Y. Yamamoto, Rev. Mod. Phys. **82**, 1489 (2010).
[43]The similar effect holds for interband polaritons, for which decoherence length is much bigger than for bare excitons. See, e.g., W. Langbein, I. A. Shelykh, D. Solnyshkov, G. Malpuech, Yu. Rubo, and A. Kavokin, Phys. Rev. B **75**, 075323 (2007).